J. Fluid Mech. (1986), *vol.* 162, *pp.* 171–186
Printed in Great Britain

A general wave equation for waves over rippled beds

By JAMES T. KIRBY

Coastal and Oceanographic Engineering Department, University of Florida, Gainesville, FL 32611 USA

(Received 2 January 1985 and in revised form 17 May 1985)

A time-dependent extension of the reduced wave equation of Berkhoff is developed for the case of waves propagating over a bed consisting of ripples superimposed on an otherwise slowly varying mean depth which satisfies the mild-slope assumption. The ripples are assumed to have wavelengths on the order of the surface wavelength but amplitudes which scale as a small parameter along with the bottom slope. The theory is verified by showing that it reduces to the case of plane waves propagating over a patch of sinusoidal ripples, which vary in one direction and extend to $\pm\infty$ in the transverse direction, studied recently by Davies & Heathershaw and Mei. We then formulate and use coupled parabolic equations to study propagation over patches of arbitrary form in order to study wave reflection.

1. Introduction

The problem of reflection of surface waves by patches of large bottom undulations has received an increasing amount of attention recently, owing to this mechanism's possible importance in the development of shore-parallel bars. Davies & Heathershaw (1984) and Mei (1985) have recently studied the case of reflection from sinusoidal topography and have provided analytic treatments which exhibit the mechanism of a resonant Bragg reflection at the point where the wavelength of the bottom undulation is one half the wavelength of the surface wave. Davies & Heathershaw provide a solution to the linear problem which employs a perturbation expansion using the ripple amplitude as the small parameter; reflected waves appear at second order as forced solutions. This theory is not valid near the Bragg-scattering condition for resonance, and Davies & Heathershaw provide a somewhat artificial correction in this region which ensures conservation of energy in the scattered wave field. On the other hand, Mei concentrated on the reflection process at or close to the resonance condition and obtained evolution equations for the dominant free-wave components. The results of both theories agree suitably well with experimental results for reflection from a finite patch of sinusoidal ripples.

Based on the analytic and experimental results, Mei suggests that reflection of waves from an initially isolated bar (such as a break-point bar formed at the outer edge of the surf zone) may be sufficient to induce the formation of bars further offshore of the initial bar, while Heathershaw (1982) has investigated and discussed the initial accretion of loose sediment and initiation of extra bars upwave of a limited barfield.

The analytic results presented to date illustrate the major features to be expected when studying reflection from a system of bars. However, they are too limited in scope to provide a direct treatment in the case of natural bed forms varying arbitrarily in two horizontal directions. For this reason, the present study concentrates on the

development of a general wave equation which is applicable to linear surface waves in intermediate or shallow water depths. The resulting equation is similar in spirit to the reduced wave equation of Berkhoff (1972), but extends the usual mild-slope approximation to include rapidly varying, small-amplitude deviations from the slowly varying mean depth, which lie outside the scope of Berkhoff's equation. The resulting equation is generally applicable both to the case of resonant scattering by an undulating bottom and to the case of slow, non-resonant scattering by detuned undulations or by the slow change in average depth, which is important in the absence of strong resonant scattering. In contrast, the results below indicate that the original mild-slope formulation is not generally applicable to the cases of resonant scattering to be studied.

After deriving the general equation in §2, we consider the correspondence between the present results and those of Mei (1985) and Long (1973) in §3. A simple numerical scheme is used to solve the reduced wave equation for the case of reflection over one-dimensional topographies, and comparisons are given between the prediction of the present theory and the corresponding results using the mild-slope approximation.

In §4 we apply a splitting method in order to reduce the elliptic form to two coupled parabolic equations for forward- and backscattered waves. The resulting equations for amplitude of the forward- and backward-propagating waves extend the results of Mei to the case of arbitrary topographic variations and include possible diffraction effects.

2. Derivation of the wave equation

The depth-integrated wave equation for monochromatic, linear waves propagating over small-amplitude bed undulations may be formulated following either a variant of the Green's formula method of Smith & Sprinks (1975) or Liu (1983), or by using the Lagrangian formulation of Kirby (1984). Here the Green's formula approach is utilized.

Let $h'(\boldsymbol{x})$, $\boldsymbol{x} = \{x, y\}$, denote the total still-water depth, and let

$$h' = h(\boldsymbol{x}) - \delta(\boldsymbol{x}); \tag{2.1}$$

where $h(\boldsymbol{x})$ is a slowly varying depth satisfying the mild-slope assumption

$$\frac{\nabla_{\mathrm{h}} h}{kh} \ll 1, \quad \nabla_{\mathrm{h}} = \left\{\frac{\partial}{\partial x}, \frac{\partial}{\partial y}\right\}. \tag{2.2}$$

$\delta(\boldsymbol{x})$ represents rapid undulations of the depth about the mean level, as indicated in figure 1. We consider the problem to be linearized in wave amplitude but retain first-order terms in the bed-undulation amplitude. We assume

$$O\left(\frac{\nabla_{\mathrm{h}} h}{kh}\right) \approx O(k\delta) \ll 1. \tag{2.3}$$

Linearizing the free-surface boundary conditions and expanding the bottom boundary condition about $z = -h$, we obtain to $O(k\delta)$

$$\nabla_{\mathrm{h}}^2 \phi + \phi_{zz} = 0 \quad (-h \leqslant z \leqslant 0), \tag{2.4}$$

$$\phi_{tt} + g\phi_z = 0 \quad (z = 0), \tag{2.5}$$

$$\phi_z = -\nabla_{\mathrm{h}} h \cdot \nabla_{\mathrm{h}} \phi + \nabla_{\mathrm{h}} \cdot (\delta \nabla_{\mathrm{h}} \phi) \quad (z = -h) \tag{2.6}$$

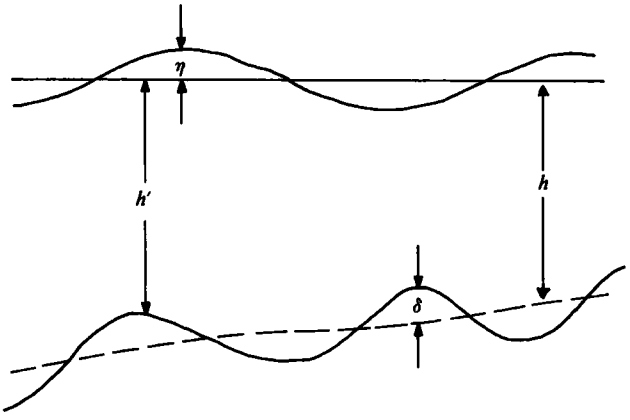

FIGURE 1. Definition of depth components.

Equation (2.6) has been given previously by Mei (1985) and in different form by Davies & Heathershaw (1984). To leading order ($\delta \to 0$), the solution to (2.4)–(2.6) may be expressed as

$$\phi(\boldsymbol{x}, z, t) = f(\boldsymbol{x}, z)\,\tilde{\phi}(\boldsymbol{x}, t) + \Sigma \text{ non-propagating modes} + O(k\delta), \tag{2.7}$$

where $f = \cosh k(h+z)/\cosh kh$ is a slowly varying function of $\boldsymbol{x}$, and where

$$\omega^2 = gk \tanh kh \tag{2.8}$$

locally, with ω being the fixed angular frequency and k the wavenumber. We then use Green's second identity to extract the propagating component of ϕ:

$$\int_{-h}^{0} f\phi_{zz}\,\mathrm{d}z - \int_{-h}^{0} \phi f_{zz}\,\mathrm{d}z = [f\phi_z - \phi f_z]_{-h}^{0}. \tag{2.9}$$

The integrals are manipulated to obtain finally

$$\begin{aligned}\tilde{\phi}_{tt} - \nabla_{\mathrm{h}}\cdot(CC_{\mathrm{g}}\nabla_{\mathrm{h}}\tilde{\phi}) + (\omega^2 - k^2CC_{\mathrm{g}})\tilde{\phi} + gf^2|_{-h}\nabla_{\mathrm{h}}\cdot(\delta\nabla_{\mathrm{h}}\tilde{\phi}) \\ + g\int_{-h}^{0} f\nabla_{\mathrm{h}}^2 f\,\mathrm{d}z\,\tilde{\phi} + gf\nabla_{\mathrm{h}}f\cdot\nabla_{\mathrm{h}}h|_{-h}\tilde{\phi} + gf\nabla_{\mathrm{h}}f\cdot\nabla_{\mathrm{h}}\delta|_{-h}\tilde{\phi} \\ + g\delta(f\nabla_{\mathrm{h}}^2 f)|_{-h}\tilde{\phi} + 2g\delta f\nabla_{\mathrm{h}}f\cdot\nabla_{\mathrm{h}}\tilde{\phi}|_{-h} = 0,\end{aligned} \tag{2.10}$$

where $C = \omega/k$ and $C_{\mathrm{g}} = \partial\omega/\partial k$.

The last five terms are proportional to either $(\nabla_{\mathrm{h}}h)^2$ or $\delta\nabla_{\mathrm{h}}h$, and are thus second order in the small parameter. Neglecting them and substituting for $f(z=-h)$ then gives

$$\tilde{\phi}_{tt} - \nabla_{\mathrm{h}}\cdot(CC_{\mathrm{g}}\nabla_{\mathrm{h}}\tilde{\phi}) + (\omega^2 - k^2CC_{\mathrm{g}})\tilde{\phi} + \frac{g}{\cosh^2 kh}\nabla_{\mathrm{h}}\cdot(\delta\nabla_{\mathrm{h}}\tilde{\phi}) = O(k\delta)^2. \tag{2.11}$$

Equation (2.11) governs the value of the potential at the free surface for an arbitrary wave motion. Neglecting the term in δ yields a time-dependent form of Berkhoff's (1972) equation for the slowly varying bottom alone.

This completes the derivation using the Green's identity method. The derivation of a nonlinear form of (2.11) in the context of the Lagrangian formulation is given by Kirby (1986).

3. Correspondence to previous results

In order to demonstrate the completeness and generality of the wave equation (2.11), we first consider its reduction to the coupled evolution equations of Mei (1985) for resonant Bragg scattering by a finite patch of ripples. We then employ a finite-difference form of (2.11), after neglecting time dependence, to study the one-dimensional (x only) reflection for a range of incident wavelengths, and compare our results to the data presented by Davies & Heathershaw (1984). Finally, a discussion of some correspondences with the work of Long (1973) is presented.

3.1. *Resonant Bragg scattering*

Consider the particular example, studied by Davies & Heathershaw (1984) and Mei (1985), of waves propagating normally over a ripple patch varying in x and extending uniformly to $\pm\infty$ in y. Depth h is taken to be constant, while δ is given by

$$\delta = \tfrac{1}{2}D(e^{i\lambda x}+e^{-i\lambda x}) \quad (0 \leqslant x \leqslant L),$$

where $0 \leqslant x \leqslant L$ is the range of the ripple patch, and

$$\delta = 0 \quad (x < 0,\ x > L).$$

We consider an incident wave

$$\tilde{\phi}^{+} = -\frac{ig}{2\omega} A(x,t)\, e^{i(kx-\omega t)}, \tag{3.1}$$

and reflected wave

$$\tilde{\phi}^{-} = -\frac{ig}{2\omega} B(x,t)\, e^{i(-kx-\omega t)}, \tag{3.2}$$

where A and B are slowly varying functions of x and t. The conditions for resonant Bragg scattering are satisfied when the bottom undulation has a wavelength of one-half the surface wavelength, or

$$\lambda = 2k. \tag{3.3}$$

Employing this result, we proceed by assuming that derivatives of A and B are $O(k\delta)$ in comparison to A and B and keep terms only to $O(k\delta)$. Defining

$$\Omega_0 = \frac{gk^2D}{4\omega \cosh^2 kh} \tag{3.4}$$

and collecting terms of like powers in e^{ikx}, we obtain

$$A_t + C_g A_x = -i\Omega_0 B, \tag{3.5}$$

$$B_t - C_g B_x = -i\Omega_0 A, \tag{3.6}$$

which are a special case of the results of Mei, neglecting mean bottom slope and oblique angle of incidence. In the derivation of (3.5)–(3.6), we have neglected terms which couple A and B but which have rapidly oscillating coefficients, since these terms do not contribute to the direct resonance. Solutions of (3.5) and (3.6) in relation to the experimental results of Davies & Heathershaw are discussed in detail by Mei. All of Mei's subsequent results may be obtained from (2.11) following this procedure and his assumptions.

For later use, we define an unscaled frequency-like term Ω' according to

$$\Omega_0 = \Omega'(kD), \tag{3.7}$$

where $\Omega' \sim 0(1)$. Ω' will be advantageous in the general case since it is not dependent on the geometry of the undulations. (Note that Ω' may still be a slowly varying function of the mean depth.)

3.2. *One-dimensional reflection from a ripple patch*

We now test the reduced, elliptic form of (2.11) for the case of waves normally incident on a finite ripple patch. Variations in the y-direction are neglected; the resulting problem is equivalent to that studied by Davies & Heathershaw if we restrict attention to sinusoidal undulations of constant amplitude and constant mean depth h. After setting h = constant, (2.11) reduces to

$$\hat{\phi}_{xx} + k^2\hat{\phi} - 4\left(\frac{\Omega'}{C_g}\right)(\delta\hat{\phi}_x)_x = 0, \tag{3.8}$$

where

$$\tilde{\phi} = \hat{\phi}(x)\,\mathrm{e}^{-\mathrm{i}\omega t}, \tag{3.9}$$

Ω' is defined by

$$\Omega' = \frac{gk}{4\omega\cosh^2 kh} \tag{3.10}$$

following (3.7), and where we have neglected time dependence in the wave amplitude. For the case of sinusoidal bed oscillations, we may take

$$\delta = D\sin(\lambda x) \quad (0 \leqslant x \leqslant nl), \tag{3.11}$$

where $l = 2\pi/\lambda$ is the bed wavelength and n is the number of bed ripples. the Bragg-scattering condition corresponds to $2k/\lambda = 1$. Equation (3.8) is written in finite-difference form, and radiating boundary conditions are applied according to

$$\hat{\phi}_x = -\mathrm{i}k(\hat{\phi} - 2\hat{\phi}_\mathrm{I}) \quad (x_1 < 0), \tag{3.12}$$

$$\hat{\phi}_x = \mathrm{i}k\hat{\phi} \quad (x_2 > nl), \tag{3.13}$$

where

$$\hat{\phi}_\mathrm{I} = \mathrm{e}^{\mathrm{i}kx} \tag{3.14}$$

is the incident wave of unit amplitude. x_1 and x_2 represent the upwave and downwave limits of the computational grid, which may be arbitrarily close to the outer edges of the ripple patch since non-propagating modes are not accounted for. The resulting tridiagonal matrix is inverted using a double-sweep algorithm.

We first consider the experimental results of Davies & Heathershaw and compare numerical results with the cases

(i) $n = 10$, $D/h = 0.16$,

(ii) $n = 4$, $D/h = 0.32$.

Computed results for reflection coefficient $|R|$ corresponding to a reflected wave

$$\hat{\phi}_\mathrm{R} = R\,\mathrm{e}^{-\mathrm{i}kx} \quad (x < 0) \tag{3.15}$$

are given by the solid curves in figures 2 and 3 for cases 1 and 2 respectively, in comparison to the laboratory data. Solutions were obtained using a grid spacing of $\Delta x = l/20$ in order to obtain accurate results at large $2k/\lambda$. The numerical results are nearly indistinguishable from the analytic results of Davies & Heathershaw (1984) with the exception of small shifts in the positions of the peaks and zeroes of $|R|$. These shifts may be due to the neglect of non-propagating waves at the ripple-patch edges as well as the numerical errors involved in the computation scheme. The results are

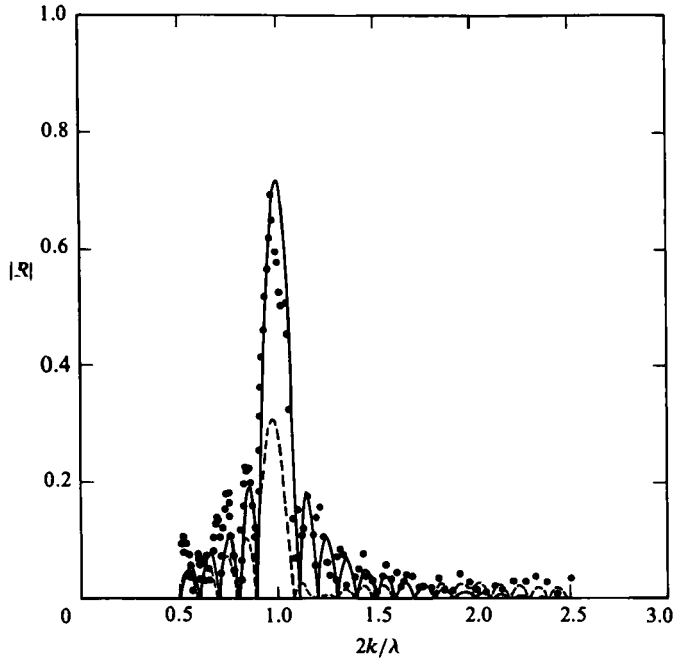

FIGURE 2. Reflection coefficient for waves normally incident on a sinusoidal patch. Case 1: $D/h = 0.16$, $n = 10$. ——, numerical results, present theory; – – –, numerical results, mild-slope theory; ●, laboratory data from Davies & Heathershaw (1984).

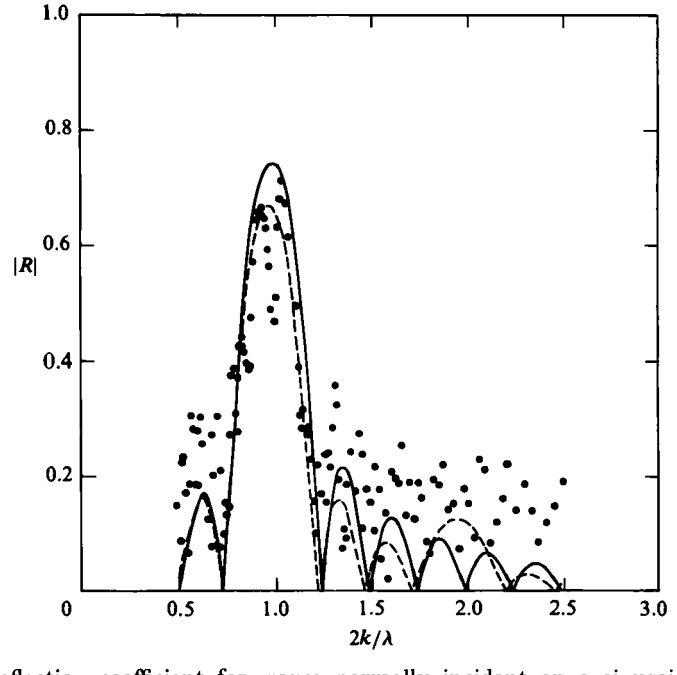

FIGURE 3. Reflection coefficient for waves normally incident on a sinusoidal patch. Case 2: $D/h = 0.32$, $n = 4$. ——, numerical results, present theory; – – –, numerical results, mild-slope theory; ●, laboratory data from Davies & Heathershaw (1984).

based on the same information as in Mei's approach, and compare well with his predictions over the range of validity of the theory for near-resonance.

Also shown in figures 2 and 3 are results obtained using the original mild-slope theory alone (dashed lines). To construct these curves, we use the one-dimensional form of Berkhoff's equation given by

$$\hat{\phi}_{xx}+\frac{1}{CC_g}(CC_g)_x\hat{\phi}_x+k^2\hat{\phi}=0, \tag{3.16}$$

where C, C_g and k are determined by the total depth $h'(x)$. In figure 2, where waves are relatively short compared to the water depth ($kh = O(1)$), a marked discrepancy is apparent between the results of the present general model and the mild-slope form of the model, with the mild-slope form clearly being unable to predict the magnitude of the resonant-reflection peak. This result may have been expected since the mild-slope equation is derived assuming that the depth must vary slowly over a wavelength. However, this is the first documented case of the mild-slope equation breaking down on a topography with local slopes less than $O(1)$, and the results indicate the utility of the new extended form of the equation.

In figure 3, the results of the mild-slope theory are in closer agreement with the results of the present generalized equation. In this case, waves are longer with respect to the average water depth, bringing us close to the shallow-water asymptote. It may be seen from inspection of (3.8) and (3.16) that both models are asymptotic to the usual linear shallow-water equation, which explains the convergence of the results as kh tends to zero.

Laboratory data from Davies & Heathershaw are included in figures 2 and 3 for comparison with the numerical results. Davies and Heathershaw provide indications of how much the data at low $|R|$ is contaminated by reflections at the end of the wave channel. The reflection effect is especially important in the figure 3 results away from the resonant peak, where data and theory are apparently not in agreement. Davies & Heathershaw indicate a reflection coefficient of about 0.2 for the beach at the end of the wave channel in this case.

As a second example, we consider the reflection of waves from a bed formed by the superposition of two Fourier components:

$$\delta = D_1 \sin\lambda x + D_2 \sin m\lambda x \quad (0 \leqslant x \leqslant 2\pi n/\lambda).$$

We consider two cases; one where both Fourier components have an integral number of wavelengths in the ripple patch, and the other where the ripple patch terminates at a half-wavelength for the second component. These cases differ since, for case one, the zeroes of the reflection coefficient for each component would separately coincide in Davies & Heathershaw's analytic treatment; while for the second case the zeroes for each component do not coincide.

For case one, we use the data of figure 3 and set $m = 2$ so that the second wave has half the wavelength of the first. Three situations are plotted in figure 4: $D_1/h = 0.32$, $D_2/h = 0$ (as in figure 3); $D_1/h = 0$, $D_2/h = 0.32$ (all variance at the shorter wavelength); and $D_1/h = D_2/h = 0.32$ (equal bottom-component amplitudes). The composite bottom is seen to produce nearly the same zeroes in $|R|$, and a peak in $|R|$ associated with resonance with each component of the bottom is apparent. As in the case of single bottom component, the shifts in positions of the zeroes may again be due both to neglect of forced, non-propagating wave modes and to numerical error. The two resonance peaks remain separate and clearly distinguishable.

For the second case, we use $n = 4$ and $m = \frac{15}{8}$, so that the second component has

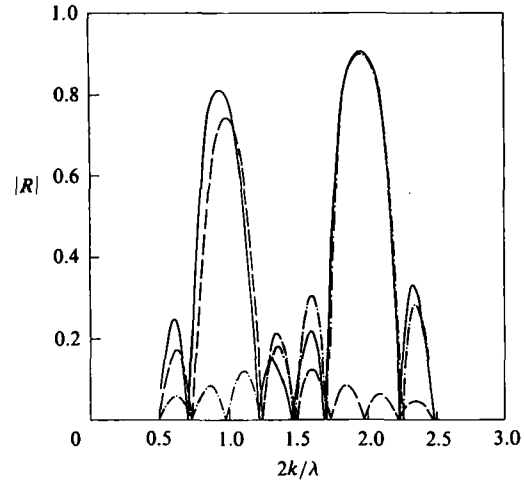

FIGURE 4. Reflection from a patch with two Fourier components, $\delta = D_1 \sin \lambda x + D_2 \sin 2\lambda x$, $n = 4$. – – –, $D_1/h = 0.32$, $D_2/h = 0$; – · – ·, $D_1/h = 0$, $D_2/h = 0.32$; ——, $D_1/h = D_2/h = 0.32$.

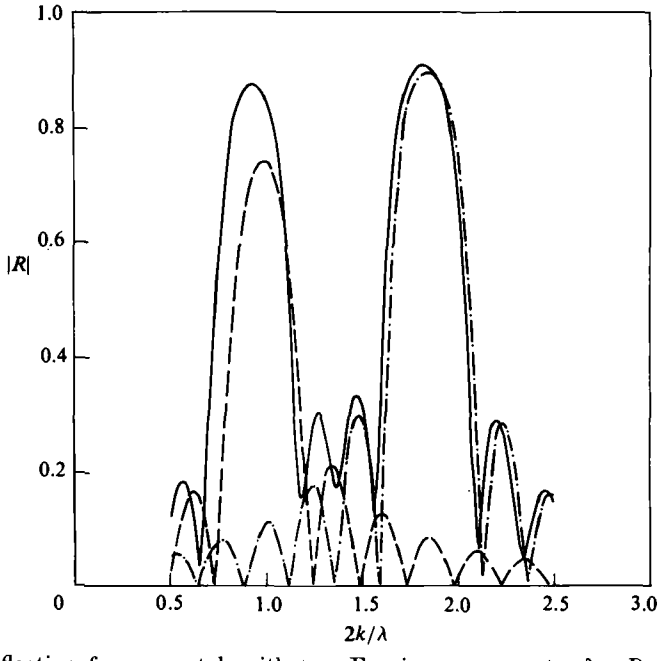

FIGURE 5. Reflection from a patch with two Fourier components, $\delta = D_1 \sin \lambda x + D_2 \sin(\frac{15}{8}\lambda x)$, $n = 4$. – – –, $D_1/h = 0.32$, $D_2/h = 0$; – · –, $D_1/h = 0$, $D_2/h = 0.32$; ——, $D_1/h = D_2/h = 0.32$.

$7\frac{1}{2}$ wavelengths in the ripple patch. Curves of $|R|$ for the same three distributions of ripple amplitudes as described above are given in figure 5. Now the reflection coefficients associated with each component acting separately have different zeroes. The two patterns together interact and destroy the zeroes; the resulting curve of $|R|$ varies smoothly over the range of $2k/l$ considered. The peaks associated with resonant scattering from each component are again distinct and strong.

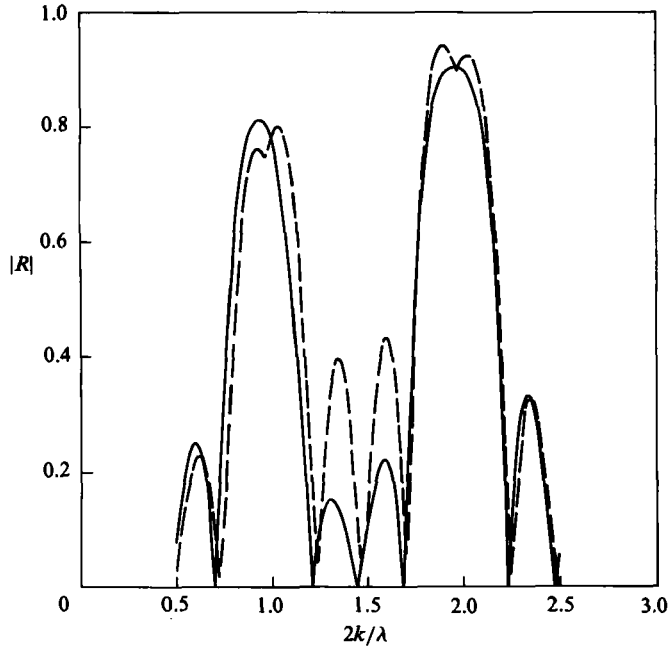

FIGURE 6. Reflection from a patch with two Fourier components $\delta = D_1/\sin\lambda x + D_2 \sin 2\lambda x$, $n = 4$. ——, $D_1/h = D_2/h = 0.32$ (as in figure 5). – – –, sum of individual results for $D_1/h = 0.32$, $D_2/h = 0$ and $D_1/h = 0$, $D_2/h = 0.32$.

Figure 6 shows a comparison between the reflection coefficient for the composite bottom of figure 4, and an artificially constructed reflection coefficient obtained by simply summing the individual reflection coefficients for the two bottom components of figure 4 acting separately. Agreement between the actual and artificial reflection coefficients is fairly close near the resonance peaks, where one bottom component dominates, but they become quite different away from any resonance, indicating a significant mutual interaction between all wavelike features away from a dominant resonance.

The strength of resonant reflection from an organized barfield implies that a broad spectrum, containing a band of wavelengths which are nearly or exactly resonant with the bottom, may experience fairly significant reduction in energy density near the resonance wavenumber. Further, the reflected wave field, which may assume the form of a fairly narrow spectral band around the resonant wavenumber, may be much 'groupier' than the incident-wave field. This groupiness may lead to significant forced long-wave motions propagating in the offshore direction. These motions would be similar in form to the offshore-propagating long wave caused by wave-group pumping of the surf zone (studied recently by Symonds & Bowen 1984; and Symonds, Huntley & Bowen 1982), but do not require the incident-wave field to be distinctly groupy in nature.

Unfortunately, no laboratory data exists to test these hypotheses; verification of the present results and conjectures thus require further independent effort.

3.3. *Scattering by a random bottom; comparison with Long's* (1973) *results*

Long (1973) has presented a model for the scattering of surface waves by irregular bottom variations, which is based on the perturbation scheme of Hasselmann (1966).

Long's study generalizes the Bragg-scattering problem considered here to the problem of interaction between a directional spectrum of random surface waves interacting with a directional spectrum of bottom variations. He shows that the generalization of the Bragg condition to waves oriented at any angle to a relevant bottom component is given by

$$\boldsymbol{k}''(\theta'') = \boldsymbol{k}(\theta) - \boldsymbol{k}'(\theta'), \tag{3.17}$$

where $\boldsymbol{k}''$ is the wavenumber vector of a spectral component of the bottom, $|\boldsymbol{k}| = |\boldsymbol{k}'| = k$ are the magnitudes of the wavenumbers of the two surface-wave components at equal frequency, and θ and θ' are the directions of propagation of the surface components with respect to a reference direction. The resonance condition gives

$$k'' = |\boldsymbol{k}''| = 2^{\frac{1}{2}} k(1-\cos(\theta-\theta'))^{\frac{1}{2}}, \tag{3.18}$$

$$\theta'' = \tfrac{1}{2}(\theta+\theta') \pm \tfrac{1}{2}\pi. \tag{3.19}$$

In this case, Hasselmann's general interaction equation specializes to

$$\frac{\partial F(\boldsymbol{k})}{\partial t} = \sum_{k'>0} \iint \mathrm{d}^2 k'\, 16\pi\, |3\omega D_{-kk'k''}|^2\, F_{\mathrm{b}}(\boldsymbol{k}'') \cdot (F(\boldsymbol{k}') - F(\boldsymbol{k})), \tag{3.20}$$

which is Long's equation (1). Here, $F(\boldsymbol{k})$ and $F(\boldsymbol{k}')$ are the spectral densities of the surface waves in the θ and θ' directions, and $F_{\mathrm{b}}(\boldsymbol{k}'')$ is the spectral density of the bottom variations in direction θ'' with wavenumber k'' given by (3.18). In (3.20), $D_{-kk'k''}$ is given by (Long)

$$D_{-kk'k''} = -\frac{\boldsymbol{k}\cdot\boldsymbol{k}'}{6k \sinh kh \cos kh}. \tag{3.21}$$

Specializing to the case studied in §3.1, we may restrict attention to the case where

$$\boldsymbol{k}' = -\boldsymbol{k},$$

where

$$\boldsymbol{k}'' = \boldsymbol{\lambda} = 2\boldsymbol{k}.$$

In this case, the transfer coefficient in (3.20) reduces to

$$|3\omega D|^2 = 4k^2\Omega'^2$$

in our notation. Long's model then predicts that the rate of change of the energy density of a single wave component is proportional to the difference between the densities of the interacting pair of surface waves.

Neglecting the spatial dependence of the amplitude components A and B in (3.5) and (3.6), these equations may be manipulated (together with their complex conjugates) to give

$$|A|_t^2 = -\mathrm{i}\Omega_0(A^*B - AB^*), \tag{3.22a}$$

$$|B|_t^2 = \mathrm{i}\Omega_0(A^*B - AB^*), \tag{3.22b}$$

which indicates that

$$(|A|^2 + |B|^2)_t = 0; \tag{3.23}$$

energy is conserved by the interaction (see Mei for a more extensive discussion). In order to get equations which are closer in form to Long's equation, we may differentiate (3.22) with respect to time again and then use (3.5) and (3.6) to eliminate time derivatives from the resulting right-hand sides; we get

$$|A|_{tt}^2 = 2\Omega_0^2(|B|^2 - |A|^2), \tag{3.24a}$$

$$|B|_{tt}^2 = 2\Omega_0^2(|A|^2 - |B|^2). \tag{3.24b}$$

From this pair we see that the rate of change of the growth rate of the energy density is proportional to the differences in energy densities of the interacting components, in contrast to the results of Long, where only the growth rate itself is involved. Equations (3.24) indicate the possibility of a slow reversal phenomenon, where a dominant wave travelling in one direction is gradually replaced by a dominant wave travelling in the opposite direction (Mitra & Greenberg 1984). In particular, for an initial condition $|A|^2(0) = A_0^2$ and $|B|^2(0) = 0$; i.e. a purely progressive wave, (3.24) has the solution

$$|A|^2(t) = \tfrac{1}{2}A_0^2(1+\cos 2\Omega_0 t), \tag{3.25a}$$

$$|B|^2(t) = \tfrac{1}{2}A_0^2(1-\cos 2\Omega_0 t), \tag{3.25b}$$

indicating a complete transfer of energy from the initial wave to the resonantly forced reflected wave, after which the process repeats cyclically. Long's model, on the other hand, would indicate a final equilibration of the forward- and backward-travelling spectral densities.

4. Coupled parabolic equations for forward- and back-scattered waves

We now consider the development of coupled parabolic equations for forward- and back-scattered waves, following the results of Radder (1979) and Liu & Tsay (1983). The goal is to obtain an extension to the refraction results of Mei (1985) (as in (3.5) and (3.6)) to cover cases where δ varies arbitrarily in x and y, and where y-variations in δ or h may induce sufficiently strong amplitude variations to warrant the introduction of diffraction effects. We take x to correspond to a principal propagation direction and assume that deviations from this direction are small. Neglecting time dependence in the wave amplitude, (2.11) may be written in elliptic form as

$$p\hat{\phi}_{xx} + p_x\hat{\phi}_x + k^2CC_g\hat{\phi} + (CC_g\hat{\phi}_y)_y - \frac{4\omega\Omega'}{k}(\delta\hat{\phi}_y)_y = 0, \tag{4.1}$$

where

$$p = CC_g - \frac{4\omega\Omega'\delta}{k}. \tag{4.2}$$

(4.1) may then be written as

$$\hat{\phi}_{xx} + p^{-1}p_x\hat{\phi}_x + k^2CC_gp^{-1}\hat{\phi} + p^{-1}(CC_g\hat{\phi}y)_y - \frac{4\omega\Omega'p^{-1}}{k}(\delta\hat{\phi}_y)_y, \tag{4.3}$$

where, to leading order in $(k\delta)$, p^{-1} is given by

$$p^{-1} = (CC_g)^{-1}\left\{1+4\left(\frac{\Omega'}{C_g}\right)\delta + O(k\delta)^2\right\}. \tag{4.4}$$

Next we denote an operator $\gamma^2\phi$ according to

$$\gamma^2\phi = k^2CC_gp^{-1}\phi + p^{-1}(CC_g\phi_y)_y - \frac{4\omega\Omega'p^{-1}}{k}(\delta\phi_y)_y,$$

or

$$\gamma^2\phi = k^2\left\{\left(1+4\frac{\Omega'}{C_g}\delta\right)\phi + \frac{1}{k^2CC_g}(CC_g\phi_y)_y - \frac{4}{k^2}\frac{\Omega'}{C_g}(\delta\phi_y)_y\right\} + O(k\delta)^2. \tag{4.5}$$

The corresponding pseudo-operator $\gamma\phi$ is obtained by expanding the square root to give

$$\gamma\phi = k\left\{\left(1+2\frac{\Omega'}{C_g}\delta\right)\phi + \frac{1}{2k^2CC_g}(CC_g\phi_y)_y - \frac{2}{k^2}\frac{\Omega'}{C_g}(\delta\phi_y)_y\right\} + O(k\delta)^2. \tag{4.6}$$

We now follow a simple scheme for obtaining the coupled parabolic equations. Let $\hat{\phi}$ be expressed as the sum of forward- and backward-propagating waves:

$$\hat{\phi} = \phi^+ + \phi^-. \tag{4.7}$$

We then assume the coupled equations:

$$\phi_x^+ = \mathrm{i}\gamma\phi^+ + F(\phi^+, \phi^-), \quad \phi_x^- = -\mathrm{i}\gamma\phi^- - F(\phi^+, \phi^-), \tag{4.8}$$

where the coupling term F is unknown. Repeated substitution of (4.8) in (4.3) finally yields

$$F(\phi^+, \phi^-) = -\frac{(\gamma p)_x}{2\gamma p}(\phi^+ - \phi^-), \tag{4.9}$$

which may be expanded to give

$$F(\phi^+, \phi^-) = -\left\{\frac{(kCC_g)_x}{2kCC_g} - \left(\frac{\Omega'}{C_g}\right)\delta_x\right\}(\phi^+ - \phi^-) \tag{4.10}$$

to leading order in $(k\delta)$. The coupled equations in expanded form are given by

$$\phi_x^+ = \mathrm{i}k\left\{1 + 2\left(\frac{\Omega'}{C_g}\right)\delta\right\}\phi^+ + \frac{\mathrm{i}}{2kCC_g}(CC_g\phi_y^+)_y$$
$$-\frac{2\mathrm{i}}{k}\left(\frac{\Omega'}{C_g}\right)(\delta\phi_y^+)_y - \frac{(kCC_g)_x}{2kCC_g}(\phi^+ - \phi^-) + \left(\frac{\Omega'}{C_g}\right)\delta_x(\phi^+ - \phi^-); \tag{4.11}$$

$$\phi_x^- = -\mathrm{i}k\left\{1 + 2\left(\frac{\Omega'}{C_g}\right)\delta\right\}\phi^- - \frac{\mathrm{i}}{2kCC_g}(CC_g\phi_y^-)_y$$
$$+\frac{2\mathrm{i}}{k}\left(\frac{\Omega'}{C_g}\right)(\delta\phi_y^-)_y + \frac{(kCC_g)_x}{2kCC_g}(\phi^+ - \phi^-) - \left(\frac{\Omega'}{C_g}\right)\delta_x(\phi^+ - \phi^-). \tag{4.12}$$

We introduce the complex amplitudes A, B according to

$$\phi^+ = -\frac{\mathrm{i}g}{\omega}A\,\mathrm{e}^{\mathrm{i}k_0 x},$$

$$\phi^- = -\frac{\mathrm{i}g}{\omega}B\,\mathrm{e}^{-\mathrm{i}k_0 x},$$

where k_0 is a reference wavenumber. (4.11) and (4.12) become

$$2\mathrm{i}kCC_g A_x + \{2k(k-k_0)CC_g + \mathrm{i}(kCC_g)_x + 2\omega\Omega'[2k\delta - \mathrm{i}\delta_x]\}A$$
$$+(CC_g A_y)_y - \frac{4\omega\Omega'}{k}(\delta A_y)_y = \{\mathrm{i}(kCC_g)_x - 2\mathrm{i}\omega\Omega'\delta_x\}B\,\mathrm{e}^{-2\mathrm{i}k_0 x}, \tag{4.13}$$

$$2\mathrm{i}kCC_g B_x + \{-2k(k-k_0)CC_g + \mathrm{i}(kCC_g)_x - 2\omega\Omega'[2k\delta + \mathrm{i}\delta_x]\}B$$
$$-(CC_g B_y)_y + \frac{4\omega\Omega'}{k}(\delta B_y)_y = \{\mathrm{i}(kCC_g)_x - 2\mathrm{i}\omega\Omega'\delta_x\}A\,\mathrm{e}^{2\mathrm{i}k_0 x}. \tag{4.14}$$

The correspondence between the present equations and the simple results of §3.1, for a one-dimensional patch of ripples and normal incidence in water of otherwise uniform depth, may be seen by substituting for δ in (4.13)–(4.14) using (3.11) and neglecting all non-resonant interactions.

The resulting equations are

$$C_g A_x - \mathrm{i}\Omega'(2k\delta - \mathrm{i}\delta_x)A = -\Omega'\delta_x B\,\mathrm{e}^{-2\mathrm{i}kx},$$
$$C_g B_x + \mathrm{i}\Omega'(2k\delta + \mathrm{i}\delta_x)B = -\Omega'\delta_x A\,\mathrm{e}^{2\mathrm{i}kx},$$

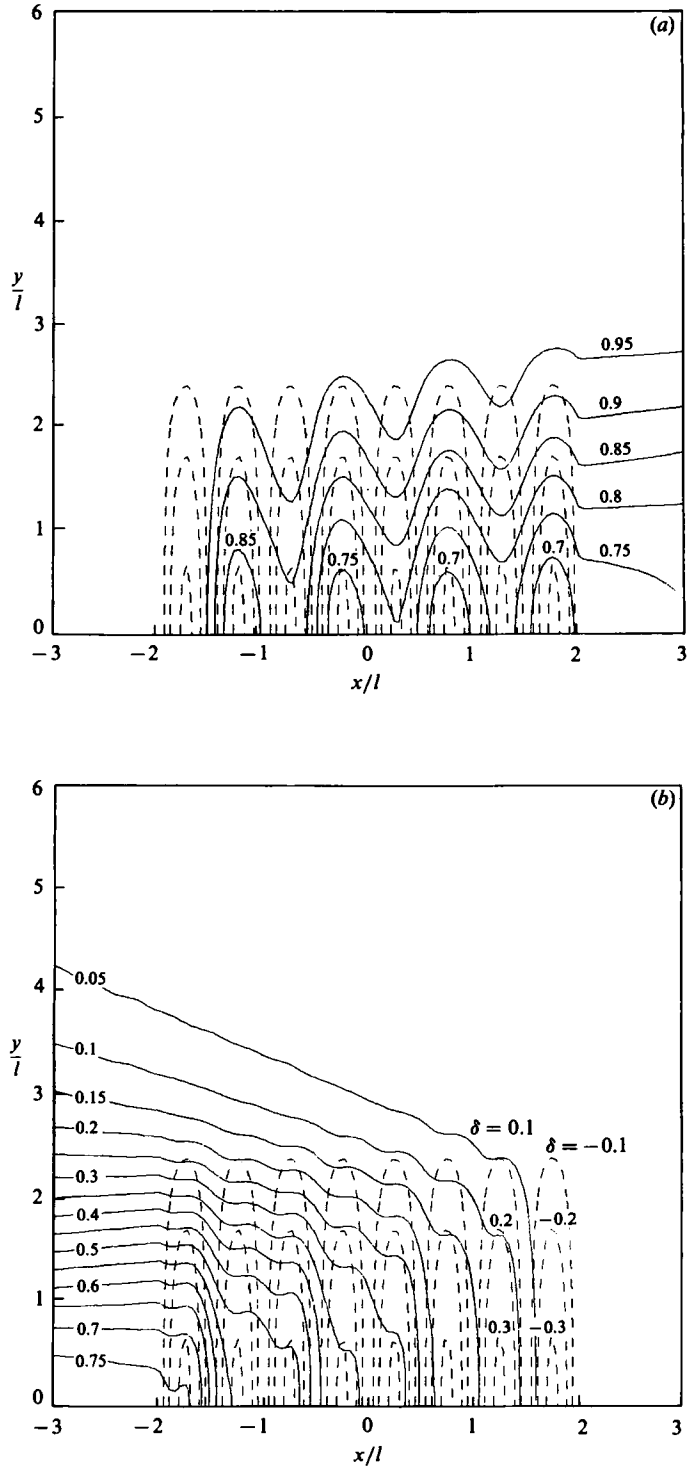

FIGURE 7 (*a*,*b*). For caption see next page.

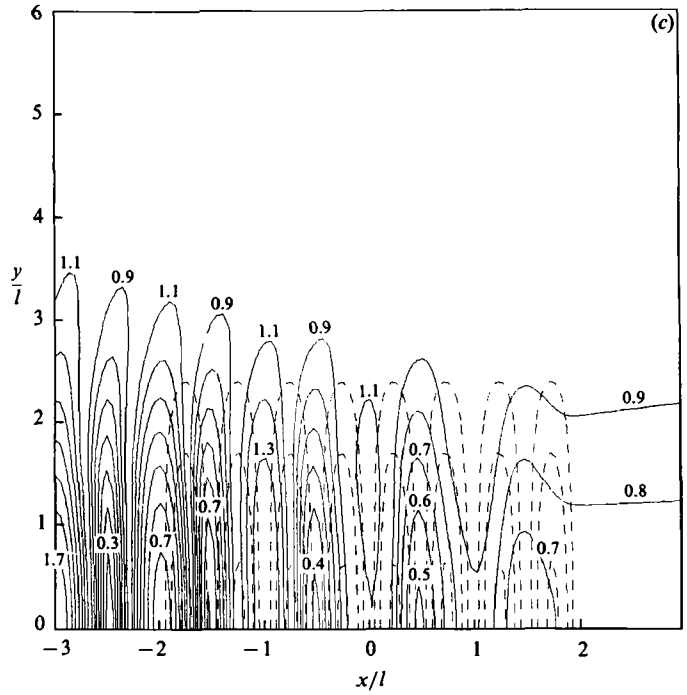

FIGURE 7. Amplitude contours with respect to incident-wave amplitude; waves propagating over two-dimensional ripple patch. (*a*) Incident wavefield $|A/A_0|$; (*b*) reflected wavefield $|B/A_0|$; (*c*) total wavefield. – – –, bottom contours; ——, amplitude contours.

or
$$\left.\begin{aligned} C_g A_x &= -\Omega_0 B \\ C_g B_x &= -\Omega_0 A \end{aligned}\right\} + \text{rapidly oscillating terms.} \qquad (4.15a,b)$$

(4.15*a*, *b*) are equivalent to (3.5)–(3.6) after neglecting time dependence and after accounting for a 90° phase shift in ripple position with respect to $x = 0$. To recover the original form, introduce a phase of $e^{\frac{1}{2}i\pi}$ in B and rewrite (4.15).

Note that the equations developed by Mei neglect diffraction effects as well as the coupling between the forward- and backward-propagating waves over the slowly varying depth. The present equations include these effects. Further, they reduce to a set of equations which are essentially similar to those of Liu & Tsay (1983) when δ is neglected.

In the following example, (4.13)–(4.14) are discretized according to the Crank–Nicolson method. The solution technique is equivalent to that used by Liu & Tsay; hence, the details are omitted here.

We construct a two-dimensional patch of ripples of finite extent in the x- and y-directions. Ripples with length l are aligned with crests parallel to the y-axis. The patch is symmetric about the x-axis and has overall dimensions of nl and $2nl$ in x and y, where n is the number of ripple wavelengths. The topography is given by h = constant and

$$\delta(x,y) = \begin{cases} D \sin(\lambda x) \cos(\lambda y/4n), & |x| \leqslant \tfrac{1}{2}nl,\ |y| \leqslant nl \\ 0, & |x| > \tfrac{1}{2}nl,\ |y| > nl. \end{cases} \qquad (4.16)$$

The computational domain is given by $-3 \leqslant x/l \leqslant 3$ and $0 \leqslant y/l \leqslant 6$. The ripples are similar to those of figure 3, with $D/h = 0.32$ and $n = 4$. Results were computed

for the resonant case $2k/\lambda = 1$ and are plotted along with the bottom contours in figure 7 (*a*) (for incident amplitude $|A|$), 7 (*b*) (for reflected amplitude $|B|$), and 7 (*c*) (for the total wavefield).

The present results were obtained using four iterations of the forward–backward calculation, which was sufficient to provide a reasonable degree of convergence. As in §3, a grid spacing of $\Delta x = \Delta y = \frac{1}{20}l$ was used. Unfortunately, no laboratory data exists to test the two-dimensional model; verification was limited to checking that results of the coupled parabolic model are equivalent to results using the elliptic model for the one-dimensional cases studied in §3.

The use of a parabolic approximation implies that wave propagation should be confined to some narrow band around the principal (x-)direction. This indicates that the amplitude contours which have spread far to the side of the ripple patch (as apparent in figures 7 (*b*, *c*)) involve some error. However, the major portion of the backscatter in this example is directly upwave along the x-axis; the spread of reflected-wave energy to the side is relatively unimportant. An indication of the amount of error in placement of amplitude contours due to over-constraint of lateral spread of energy may be obtained from Dalrymple, Kirby & Hwang (1984), who tested the parabolic equation in the context of diffraction by a semi-infinite breakwater.

5. Conclusions

This study has provided a general wave equation for linear surface waves in intermediate depth, which extends the range of applicability of the mild-slope approximation by providing for relatively rapid undulations in depth. Deviations from the mean, slowly varying depth must be small in relative amplitude but may be of any arbitrary form. The present results thus extend the previous analytic results for sinusoidal topography, and make it possible to handle directly physically realistic, one- or two-dimensional bed forms.

Although the results of §3 show that the small-amplitude theory is able to predict physically realistic results for wave reflection over bed undulations with amplitudes as large as 32 % of the mean depth, it is expected that some limitation to the present theory would occur with increasingly higher bed forms. The limitations of the small-amplitude theory are being investigated using a boundary-integral approach for bottom undulations of arbitrary height; results of this analysis will be reported separately.

This work was supported in part by the Office of Naval Research, Coastal Sciences Program. The author is grateful to Professor R. A. Dalrymple for several conversations.

REFERENCES

BERKHOFF, J. C. W. 1972 Computation of combined refraction–diffraction. In *Proc. 13th Intl Conf. Coastal Engng*, vol. 2, pp. 471–490. ASCE.

DALRYMPLE, R. A., KIRBY, J. T. & HWANG, P. A. 1984 Wave diffraction due to areas of energy dissipation. *J. Waterway, Port, Coast. and Ocean Engng* **110**, 67–79.

DAVIES, A. G. & HEATHERSHAW, A. D. 1984 Surface-wave propagation over sinusoidally varying topography. *J. Fluid Mech.* **144**, 419–443.

HASSELMANN, K. 1966 Feynmann diagrams and interaction rules of wave–wave scattering processes. *Rev. Geophys. Space Phys.* **4**, 1–32.

HEATHERSHAW, A. D. 1982 Seabed-wave resonance and sand bar growth. *Nature* **296**, 343–345.

KIRBY, J. T. 1984 A note on linear surface wave–current interaction over slowly varying topography. *J. Geophys. Res.* **89**, 745–747.

KIRBY, J. T. 1986 On the gradual reflection of weakly nonlinear Stokes waves in regions with varying topography. *J. Fluid Mech.* **162**, 187–209.

LIU, P. L.-F. 1983 Wave–current interactions on a slowly varying topography. *J. Geophys. Res.* **88**, 4421–4426.

LIU, P. L.-F. & TSAY, T.-K. 1983 On weak reflection of water waves. *J. Fluid Mech.* **131**, 59–71.

LONG, R. B. 1973 Scattering of surface waves by an irregular bottom. *J. Geophys. Res.* **78**, 7861–7870.

MEI, C. C. 1985 Resonant reflection of surface water waves by periodic sand-bars. *J. Fluid Mech.* **152**, 315–335.

MITRA, A. & GREENBERG, M. D. 1984 Slow interactions of gravity waves and a corrugated sea bed. *Trans. ASME* E: *J. Appl. Mech.* **51**, 251–255.

RADDER, A. C. 1979 On the parabolic equation method for water wave propagation. *J. Fluid Mech.* **95**, 159–176.

SMITH, R. & SPRINKS, T. 1975 Scattering of surface waves by a conical island. *J. Fluid Mech.* **72**, 373–384.

SYMONDS, G. & BOWEN, A. J. 1984 Interactions of nearshore bars with incoming wave groups. *J. Geophys. Res.* **89**, 1953–1959.

SYMONDS, G., HUNTLEY, D. A. & BOWEN, A. J. 1982 Two-dimensional surf beat: long wave generation by a time-varying breakpoint. *J. Geophys. Res.* **87**, 492–498.